Polaron physics and crossover transition in magnetite probed by pressure-dependent infrared spectroscopy

J Ebad-Allah[1], L Baldassarre[1], M Sing[2], R Claessen[2], V A M Brabers[3] and C A Kuntscher[1]

[1] Experimentalphysik 2, Universität Augsburg, D-86135 Augsburg, Germany
[2] Physikalisches Institut, Universität Würzburg, D-97074 Würzburg, Germany
[3] Department of Physics, Eindhoven University of Technology, 5600 MB Eindhoven, The Netherlands

E-mail: christine.kuntscher@physik.uni-augsburg.de

Abstract

The optical properties of magnetite at room temperature were studied by infrared reflectivity measurements as a function of pressure up to 8 GPa. The optical conductivity spectrum consists of a Drude term, two sharp phonon modes, a far-infrared band at around 600 cm^{-1} and a pronounced mid-infrared absorption band. With increasing pressure both absorption bands shift to lower frequencies and the phonon modes harden in a linear fashion. Based on the shape of the MIR band, the temperature dependence of the dc transport data, and the occurrence of the far-infrared band in the optical conductivity spectrum, the polaronic coupling strength in magnetite at room temperature should be classified as intermediate. For the lower energy phonon mode an abrupt increase of the linear pressure coefficient occurs at around 6 GPa, which could be attributed to minor alterations of the charge distribution among the different Fe sites.

1. Introduction

Magnetite (Fe_3O_4) belongs to the major class of highly correlated electron systems and shows many interesting physical properties, which have triggered a large number of experimental and theoretical investigations over the last 60 years. Fe_3O_4 has an inverse cubic spinel structure at ambient conditions and is in a mixed-valence state described as $[Fe^{3+}]_A[Fe^{2+} + Fe^{3+}]_BO_4$, where A and B denote the tetrahedral and octahedral sites, respectively, in the spinel structure AB_2O_4, with space group $Fd\bar{3}m$ [1]. Most of the proposed conduction mechanisms in magnetite are based on either band or polaron hopping motion of the extra electron through the octahedral sites occupied by Fe^{2+} and Fe^{3+} ions [2–4]. Magnetite undergoes a Verwey transition at $T_v \approx 120$ K at ambient pressure towards an insulating state [5]. On cooling through the transition temperature, the dc conductivity drops by two orders of magnitude, concurrent with a first-order structural phase transition from cubic to monoclinic symmetry [6–9]. The presence of the mixed-valent Fe ions on the B sites motivated Verwey and others [10] to hypothesize that above T_v electronic exchange takes place, whereas below T_v the transition is related to charge ordering (CO) in the mixed-valent oxide. Recent resonant x-ray diffraction experiments have specified the charge disproportionation for $T < T_v$ as $[Fe^{3+}]_A[Fe^{2.5+\delta} + Fe^{2.5-\delta}]_BO_4$, with $\delta_{12} = 0.12 \pm 0.025$ for one kind of Fe atom and $\delta_{34} = 0.1 \pm 0.06$ for another kind [11–14].

In contrast, based on Mössbauer and powder x-ray diffraction studies [12–15] it was claimed that while cooling down at ambient pressure a coordination crossover (CC) takes place at around T_v, where the spinel structure changes from inverse to normal:

$$[Fe^{3+}]_A[Fe^{2.5+} + Fe^{2.5+}]_BO_4 \rightarrow [Fe^{2+}]_A[Fe^{3+} + Fe^{3+}]_BO_4. \quad (1)$$

Within this scenario, T_{CC} increases with increasing pressure and reaches room temperature (RT) at ≈6 GPa, while T_v decreases with increasing pressure [13, 14]. Concomitant with the CC transition a small change in the pressure dependence of the tetrahedral and octahedral volumes was observed at around 6 GPa at RT, but no resolvable change in the spinel-type crystal structure or unit cell volume [14, 16, 17]. Furthermore, the hyperfine interaction parameters as a function of pressure show an anomaly at ≈7 GPa, associated with a pressure-induced discontinuous change of the Fe–O bond length [15]. The proposed valence transition from inverse to normal type is sluggish in character and hence spread over the pressure range 7–15 GPa at RT [14].

The proposal of the occurrence of a CC transition in magnetite at RT has been recently discussed based on a pressure-dependent thermoelectric power study combined with electrical resistance and sample contraction measurements [18] and a high-pressure x-ray magnetic circular dichroism study [19]. The results of both investigations exclude an inverse-to-normal spinel transition up to 20 GPa. Furthermore, in [18] a new pressure-induced crossover near 6 GPa was proposed, with either a pressure-induced 'perfection' of the electronic transport via mobile polarons, or a pressure-induced driving of the dominant inverse spinel configuration to an 'ideal' inverse spinel.

In the present work we carried out infrared reflectivity measurements to study the electronic and vibrational properties of magnetite as a function of pressure at RT. The goal of our study was twofold: first, to confirm the polaronic character of the electronic transport by monitoring the typical spectral signatures of polarons in the infrared frequency range as a function of pressure, and second, to test the proposed scenarios for the crossover transition at ∼6 GPa based on the changes in the spectral features around this critical pressure.

2. Experiment

Single crystals of magnetite used in this work were prepared from α-Fe_2O_3 using a floating-zone method with radiation heating [20]. The quality of the crystals was checked by electrical transport measurements, showing a sharp increase of the resistivity by a factor of about 100 at the critical temperature $T_v \approx 122$ K, which is characteristic for the Verwey transition (see figure 1). Furthermore, the RT value of ρ compares well with earlier reports [4, 21, 22].

In the pressure-dependent studies a clamp diamond anvil cell (Diacell cryoDAC-Mega) equipped with type IIA diamonds, which are suitable for infrared measurements, was used for the generation of pressures up to 8 GPa. Finely ground CsI powder was chosen as quasi-hydrostatic pressure medium. The single crystal was polished to a thickness of ≈50 μm and a small piece (about 140 μm × 140 μm) was cut for each pressure measurement and placed in the hole of the CuBe gasket. The pressure in the diamond anvil cell was determined by the ruby luminescence method [23].

Pressure-dependent reflectance measurements were conducted at RT from 200 cm^{-1} to 18 000 cm^{-1} using a Bruker IFS 66v/S Fourier transform infrared (FT-IR) spectrometer,

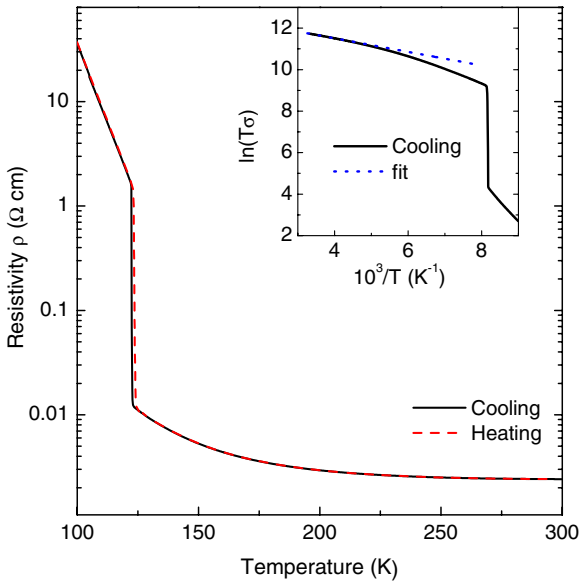

Figure 1. DC resistivity ρ as a function of temperature. Inset: Arrhenius plot and fit (dotted line) of $\ln(T\sigma)$ between 250 and 300 K according to equation (4) for small polaron hopping.

with a frequency resolution of 1 cm^{-1}, 4 cm^{-1}, and 8 cm^{-1} for the far-infrared, mid-infrared, and near-infrared/visible frequency range, respectively. To focus the beam on the small sample in the pressure cell, an infrared microscope (Bruker IRscope II) coupled to the spectrometer and equipped with a 15× magnification objective was used. The far-infrared measurements were carried out at the infrared beamline of the synchrotron radiation source ANKA, where the same equipment is installed. Reflectance spectra were measured at the interface between the sample and the diamond anvil. Spectra taken at the gasket–diamond interface served as the reference for normalization of the sample spectra. Variations in the synchrotron source intensity were taken into account by applying additional normalization procedures. The reflectivity spectra are affected in the frequency range from 1800 to 2670 cm^{-1} by multi-phonon absorptions in the diamond anvils, which are not completely corrected by the normalization procedure. This part of the spectrum was interpolated based on the Drude–Lorentz fitting. All reflectance spectra shown in this paper refer to the absolute reflectance at the sample–diamond interface, denoted as $R_{s\text{-}d}$. The reflectance spectrum of the free-standing sample (see figure 2(a)) was found to be in good agreement with earlier results [4, 26].

The real part of the optical conductivity σ_1, which directly shows the induced excitations in a material, was obtained via Kramers–Kronig (KK) transformation: to this end, the measured reflectivity data were extrapolated to low frequencies with a Drude–Lorentz fit, while data from [4] were merged at high frequencies. As an example, we show in figure 2(b) the conductivity spectrum of the free-standing sample. The value at zero frequency is consistent with the corresponding dc resistivity value (see figure 1). Regarding the high-pressure reflectance data, the sample–diamond interface was taken into account when

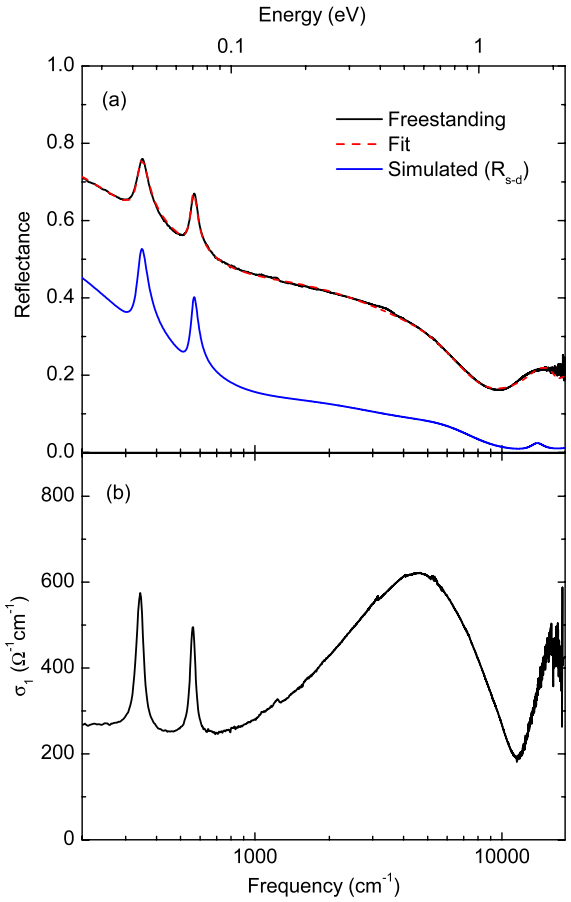

Figure 2. (a) Reflectance spectrum of free-standing magnetite, together with the Drude–Lorentz fit and the corresponding simulated reflectance spectrum $R_{s\text{-}d}$ for the sample–diamond interface, as expected in the DAC; (b) corresponding real part of the optical conductivity obtained via KK analysis.

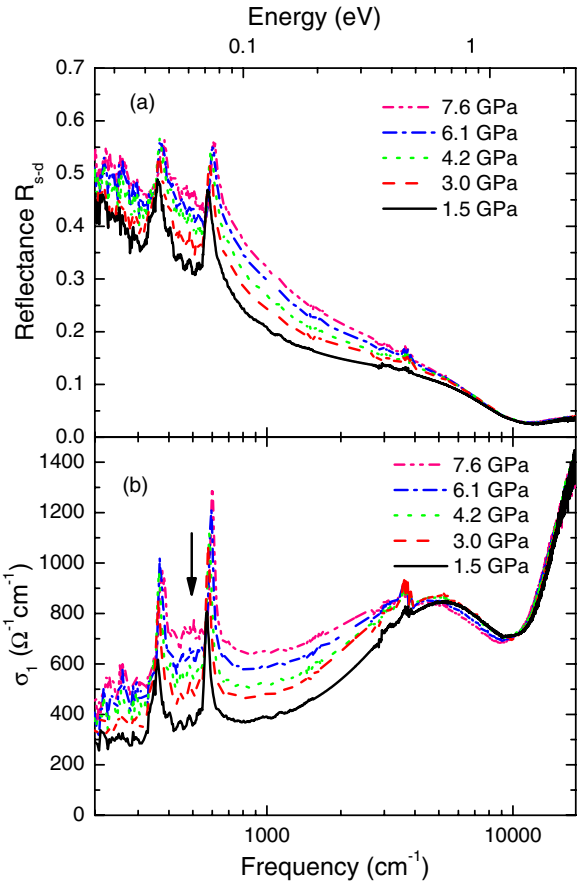

Figure 3. (a) Pressure-dependent reflectance at RT and (b) pressure-dependent real part of the optical conductivity at RT obtained by KK analysis. The arrow in (b) marks the far-infrared band as discussed in the text. The small features at around 3600 cm^{-1} are artifacts due to multi-phonon absorptions in the diamond anvil.

performing the KK analysis, as described in [27]. Overall, the level of the reflectance spectrum is lowered when switching from the sample–air to the sample–diamond interface. This is illustrated in figure 2(a) which also shows the Drude–Lorentz fit of the reflectance spectrum of the free-standing sample together with the corresponding simulated reflectance spectrum $R_{s\text{-}d}$ for the sample–diamond interface, as expected in the DAC.

3. Results

The infrared reflectance spectrum and the corresponding real part of the optical conductivity of Fe_3O_4 as a function of pressure at RT are presented in figure 3. With increasing pressure, the reflectance increases monotonically for frequencies below 5000 cm^{-1} (≈0.6 eV), indicating a growth of spectral weight within this frequency range. In contrast, the reflectance is basically pressure independent above 12 000 cm^{-1} (≈1.5 eV) [28]. We observe two T_{1u} oxygen phonon modes near 355 cm^{-1} and 565 cm^{-1}, consistent with earlier reports [4, 24–26]. The higher-frequency mode is attributed to the stretching of the A–O bond, whereas the lower-frequency mode is related to the motion of the oxygen perpendicular to this bond [29, 30]. The real part of the optical conductivity of Fe_3O_4 is presented in figure 3(b) for various pressures. The finite conductivity in the far-infrared range suggests a Drude-type contribution, indicating a metallic-like character of magnetite already at low pressure. There is a pronounced mid-infrared (MIR) absorption band located at around 5000 cm^{-1} (≈0.6 eV), which is a typical signature of polaronic excitations [31–35] and was attributed to the induced hopping of polaronic charge carriers between the Fe^{2+} and Fe^{3+} ions on the octahedral sites in magnetite [4]. An additional far-infrared band is observed in the optical conductivity spectrum at around 600 cm^{-1}, whose nature is discussed in section 4.1.

To better quantify the changes of the optical conductivity with increasing pressure, we fitted the conductivity spectra with the Drude–Lorentz model simultaneously with the reflectance spectra. The MIR band was modeled by two Lorentzian functions and the far-infrared band at around 600 cm^{-1} was described by one Lorentzian oscillator. As examples, we show in figure 4 the fitting of the optical conductivity σ_1 at $P = 1.5$ and 7.6 GPa including the various contributions, i.e., Drude term, two phonon modes, far-infrared band, MIR band, and higher-energy interband

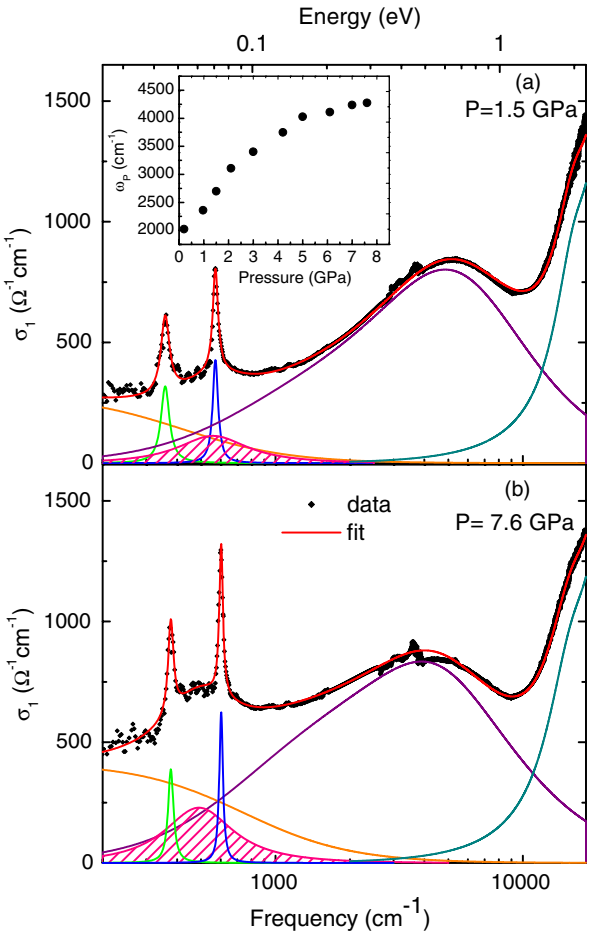

Figure 4. Fit of the RT optical conductivity σ_1 at (a) 1.5 GPa and (b) 7.6 GPa using the Drude–Lorentz model. The far-infrared band is highlighted by hatching. Inset: Plasma frequency ω_P of the Drude term as a function of pressure obtained from the Drude–Lorentz fitting.

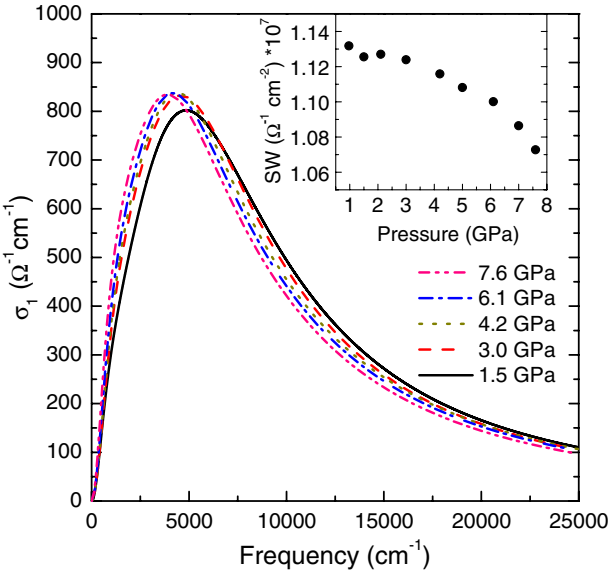

Figure 5. MIR band as a function of pressure obtained by Drude–Lorentz fitting of the optical conductivity spectra. Inset: spectral weight of the MIR band as a function of pressure.

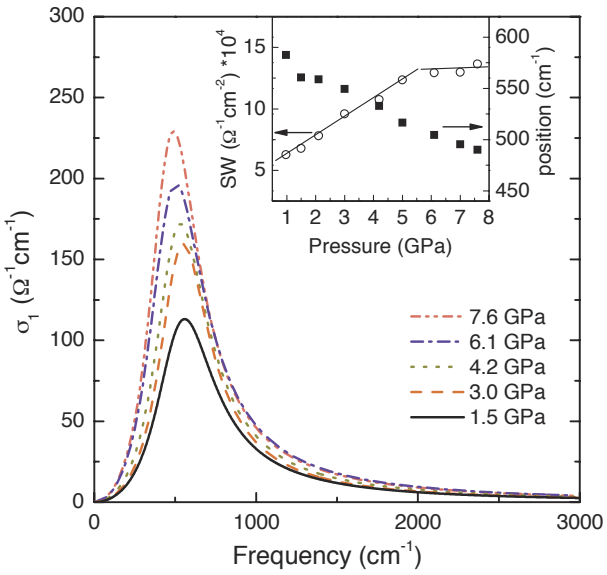

Figure 6. Far-infrared band for selected pressures, obtained by Drude–Lorentz fitting of the optical conductivity spectra. Inset: position and spectral weight of the far-infrared band as a function of pressure. Lines are guides to the eye.

transitions. By this way we were able to extract the contributions for each pressure applied.

With increasing pressure the MIR absorption band slightly narrows and redshifts, while its spectral weight [SW $= \int \sigma_1(\omega')\mathrm{d}\omega'$] decreases with increasing pressure (see inset of figure 5). The observed redshift confirms the polaronic nature of the band: according to polaron theory [36] the frequency of the polaron band is a measure of the polaron binding energy and thus of the electron–phonon coupling. In general, the electron–phonon coupling tends to decrease under pressure as a result of the combined band broadening and stiffening of the crystal lattice. Hence, one expects a decrease of the polaron binding energy under pressure. The pressure-induced redshift of the polaronic absorption band was also observed for other transition-metal oxides [32, 37]. The evolution of the far-infrared band positioned at around 600 cm^{-1} with pressure is depicted in figure 6: it shifts monotonically to lower energy and its spectral weight increases, with a saturation above ≈6 GPa (see inset of figure 6).

The stiffening of the lattice under pressure, as mentioned above, is demonstrated by the hardening of the two phonon modes (see figure 7): Both modes shift linearly with increasing pressure. The corresponding linear pressure coefficient B was obtained by fitting the peak positions with the function $\omega(P) = A + B \times P$, where P is the applied pressure. For the higher-energy mode we obtain $B = 4.9$ cm^{-1} GPa^{-1} for the whole studied pressure range. For the lower-energy mode the linear pressure coefficient is $B = 1.9$ cm^{-1} GPa^{-1} up to ≈6 GPa; at this pressure, an abrupt enhancement of the pressure-induced hardening occurs, with $B = 4.9$ cm^{-1} GPa^{-1} for the pressure range 6–8 GPa. Interestingly, at the same pressure (≈6 GPa)

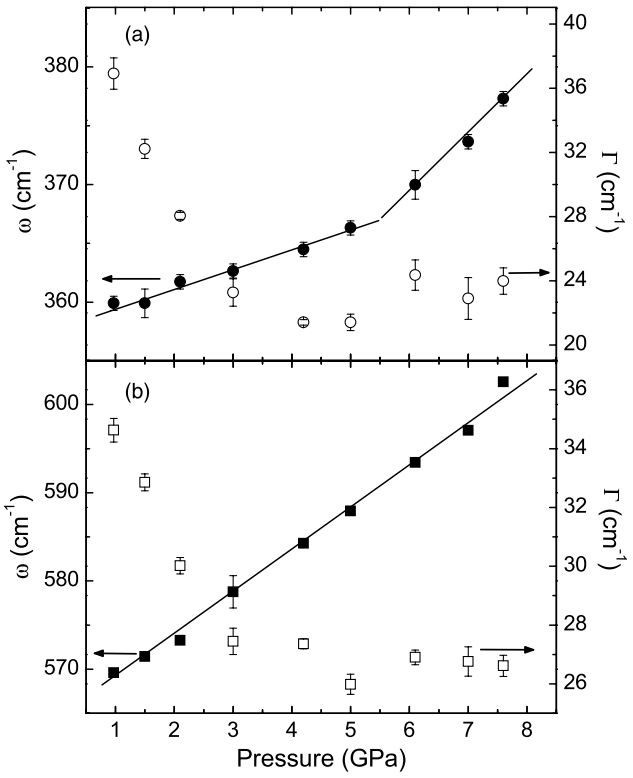

Figure 7. Phonon frequencies and linewidths as a function of pressure obtained by Drude–Lorentz fitting of the optical conductivity spectra. The lines are linear fits to the data points, in order to obtain the linear pressure coefficients.

an anomaly is found in the pressure dependence of the tetrahedral and octahedral volumes [14], the hyperfine interaction parameters [15], and the sample's contraction [18]. In addition, drastic changes are observed in the pressure dependence of the thermopower and electrical resistance near 6 GPa [18]. This issue is discussed in section 4.2.

4. Discussion

4.1. Polaronic excitations

In order to substantiate the qualitative picture of the polaronic transport in magnetite, we have analyzed the MIR absorption band in the optical conductivity data using the small polaron model. The optical properties of small polarons have recently been reinvestigated in the frame of the Holstein model using the dynamical mean-field theory [38]. In [38] both the antiadiabatic and the adiabatic regimes for the polaron formation are discussed, which are distinguished by the adiabaticity ratio $\gamma = \omega_0/D$, where ω_0 is a typical phonon frequency and D is half the free-electron bandwidth. We can estimate from our optical data the value of the adiabaticity ratio to $\gamma \approx 0.1$ by using the theoretical value [39] $D \approx 0.7$ eV (since we have $\omega_0 \approx 75$ meV). Hence, we can refer to the formula in [38] obtained in the adiabatic regime.

Furthermore, the phonon-induced broadening of the electronic levels, given by the variance s of the phonon field, compared to the electronic dispersion represented by D, is

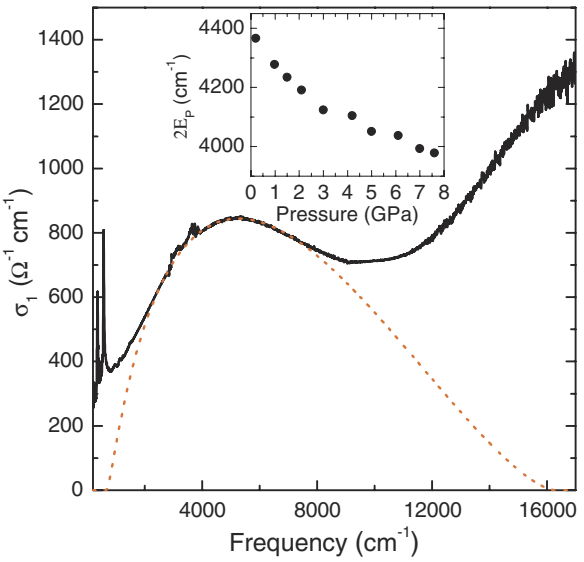

Figure 8. Fitting of the experimental optical conductivity data at 1.5 GPa using the SP model in the limit $s \ll D$ (equation (3), dotted line). The inset displays the parameter $2E_P$ as a function of pressure, obtained from the fitting using equation (3).

crucial for the shape of the polaronic optical absorption [38]. The variance s is given by [38]

$$s^2(T) = E_P \omega_0 \coth \omega_0/(2T) \qquad (2)$$

where E_P is the polaron binding energy or the ground state energy of the polaron. We estimate the value of E_P from the position of the MIR band, which is located at $\omega_{max} \approx 2E_P$ for small polaron excitations, [36, 38] and thus obtain $E_P \approx 366$ meV. With the typical phonon frequency of $\omega_0 \approx 75$ meV for magnetite, this gives $s \approx 165$ meV at RT. Thus, the phonon-induced broadening is of the same order of magnitude as the electronic band dispersion with $D \approx 700$ meV [39]. For the limit $s \ll D$, the polaronic absorption band is calculated according to [38]

$$\sigma_1(\omega) \propto \frac{1 - e^{\omega/T}}{\omega} \Phi(\omega - 2E_P) N(\omega - 2E_P), \qquad (3)$$

where the function $\Phi(\epsilon)$ is the corresponding current vertex, which can be derived by $\Phi(\epsilon) = (D^2 - \epsilon^2)/3$, and the density of states $N(\epsilon) = \frac{2}{\pi D^2}\sqrt{D^2 - \epsilon^2}$ is assumed to be semi-elliptical with the half-band width D. Within this model the maximum of the absorption band is positioned at $\omega_{max} = 2E_P - D^2/2E_P$, i.e., it is shifted to lower energies relative to $2E_P$. The experimental data are well described by equation (3) (see figure 8). With increasing pressure the fitting parameter $2E_P$ is decreased, as displayed in the inset of figure 8, reflecting the pressure-induced shift of the MIR band to lower frequencies.

A further test for the quasiparticles relevant for the transport is the temperature dependence of the dc transport data above T_v. If the conduction mechanism is due to the hopping of small polarons, one expects a thermally activated behavior of the dc conductivity according to [41]

$$T\sigma(T) \propto \exp[-E_H/(k_B T)], \qquad (4)$$

where E_H is the hopping energy. Hereby, the disorder energy is omitted, which is justified for crystalline bulk materials. The inset of figure 1 displays the corresponding Arrhenius plot. Obviously, the resulting curve does not follow a simple linear behavior. By fitting the data in the temperature range 250–300 K according to equation (4), one obtains a hopping energy $E_H = 28.5$ meV, which is a factor of ≈5 smaller than the activation energy $E_A = E_P/2$ obtained from the optical data within the small polaron model ($E_P = 271$ meV at the lowest pressure applied; see the inset of figure 8). The discrepancy is, however, reduced with decreasing temperature (see the inset of figure 1), indicating that the small polaron regime is gradually approached. Interestingly, recent hard x-ray photoemission experiments [42] also observed a gradual variation from the large polaron to the small polaron regime with decreasing temperature for the temperature range 250–330 K. We therefore conclude that the polaronic coupling strength in magnetite is intermediate and the prevailing character is temperature dependent.

For this polaron crossover regime, characteristic features are expected in the optical conductivity spectrum, namely peaks at frequencies of the order of the phonon frequencies. These peaks correspond to electronic transitions between different subbands in the polaron excitation spectrum, denoted as polaron interband transitions [38, 40]. Indeed, the optical conductivity spectrum contains a far-infrared band, which shifts to lower energy and whose spectral weight is growing with increasing pressure (see figure 6). We speculate here about the polaronic nature of this far-infrared band. The observations are similar to those in other polaronic materials, like $LaTiO_{3.41}$ and β-$Sr_{1/6}V_2O_5$ [31, 35], which were also discussed within the intermediate electron–phonon coupling regime.

4.2. Crossover at ∼6 GPa

Earlier pressure studies found an anomaly in the range 6–7 GPa in various physical quantities. This anomaly was interpreted in terms of a crossover with a rearrangement of valence electrons among the different types of Fe site, including the scenario of an inverse-to-normal spinel transition according to equation (1). In the same pressure range (≈6 GPa) we observe an enhancement of the pressure-induced hardening of the lower-frequency phonon mode. Additional information about the pressure-induced changes might be inferred from the linewidth of the phonon modes. In [26], an abrupt increase of the linewidth of several phonon modes was observed while cooling through the Verwey transition. This increase was interpreted in terms of small, non-resolvable splittings of the phonon modes due to crystal symmetry lowering. In figure 7 we show, in addition to the frequencies, the linewidths of the phonon modes as a function of pressure. For both modes the linewidth decreases as a function of pressure and is basically pressure independent above ∼4 GPa. Hence, we can exclude a pressure-induced symmetry lowering of the crystal structure, since this would lift the degeneracy of the modes, resulting in mode broadening [26].

Overall, the pressure-induced changes in the optical conductivity spectrum are minor. This observation is compatible with recent proposals of minor pressure-induced alterations of the charge distribution in magnetite, without changing the principal transport mechanism via polaron hopping motion—e.g., a pressure-induced driving of the dominant inverse spinel configuration to an 'ideal' inverse spinel [18]. Interestingly, the parameters of several contributions to the optical response saturate above ∼6 GPa (for example the plasma frequency of the Drude term or the spectral weight of the far-infrared band), which is compatible with establishing an 'ideal' inverse spinel configuration.

A similar pressure-induced rearrangement of charges between different transition-metal sites was proposed recently for β-$Na_{0.33}V_2O_5$, as revealed by anomalies in the pressure-induced shifts of infrared- and Raman-active phonon modes [37, 43]. Similar to the findings in magnetite, the charge rearrangement occurs without any change in the structural units or the crystal structure symmetry [44].

5. Summary

In summary, the optical properties of magnetite have been studied at RT as a function of pressure, supplemented by ambient-pressure dc transport measurements. The optical conductivity spectrum consists of a Drude term, two sharp phonon modes, a far-infrared band at ≈600 cm^{-1}, and a pronounced MIR absorption band, which can be ascribed to excitations of polaronic quasiparticles. With increasing pressure both absorption bands shift to lower frequencies and the phonon modes harden in a linear fashion. The shape of the MIR absorption band is well described within the small polaron model. However, according to the temperature dependence of the dc transport data the small polaron character of the charge carriers prevails only at low temperature, and therefore the polaronic coupling strength in magnetite at RT should be rather classified as intermediate. This is corroborated by the occurrence of a far-infrared band in the optical conductivity spectrum. For the lower-energy phonon mode an abrupt increase of the linear pressure coefficient occurs at around 6 GPa, which can be attributed to minor alterations of the charge distribution among the different Fe sites. This observation is consistent with a pressure-induced driving of the dominant inverse spinel configuration to an 'ideal' inverse spinel, as suggested recently [18]. The occurrence of a pressure-induced inverse-to-normal spinel transition, which was proposed based on Mössbauer and x-ray diffraction studies [12–15], seems very unlikely according to our results.

Acknowledgments

We acknowledge the ANKA Angströmquelle Karlsruhe for the provision of beamtime and thank B. Gasharova, Y.-L. Mathis, D. Moss, and M. Süpfle for assistance using the beamline ANKA-IR. Fruitful discussions with S. Fratini are gratefully acknowledged. This work was financially supported by the DFG through SFB 484.

References

[1] Sasaki S 1997 *Acta Crystallogr.* B **53** 762
[2] Ihle D and Lorenz B 1985 *J. Phys. C: Solid State Phys.* **18** L647
[3] Schrupp D, Sing M, Tsunekawa M, Fujiwara H, Kasai S, Sekiyama A, Suga S, Muro T, Brabers V A M and Claessen R 2005 *Europhys. Lett.* **70** 789
[4] Park S K, Ishikawa T and Tokura Y 1998 *Phys. Rev.* B **58** 3717
[5] Verwey E J W 1939 *Nature* **144** 327
[6] Iizumi M 1982 *Acta Crystallogr.* B **38** 2121
[7] Wright J P, Attfield J P and Radaelli P G 2001 *Phys. Rev. Lett.* **87** 266401
[8] Wright J P, Attfield J P and Radaelli P G 2002 *Phys. Rev.* B **66** 214422
[9] Senn M S, Wright J P and Attfield J P 2012 *Nature* **481** 173
[10] 1980 *Phil. Mag.* B **42** 325 (Special issue)
[11] Nazarenko E, Lorenzo J E, Hodeau Y L, Mannix D and Marin C 2006 *Phys. Rev. Lett.* **97** 056403
[12] Rozenberg G Kh, Pasternak M P, Xu W M, Amiel Y, Hanfland M, Amboage M, Taylor R D and Jeanloz R 2006 *Phys. Rev. Lett.* **96** 045705
[13] Pasternak M P, Xu W M, Rozenberg G Kh, Taylor R D and Jeanloz R 2003 *J. Magn. Magn. Mater.* **265** L107
[14] Rozenberg G Kh, Amiel Y, Xu W M, Pasternak M P, Jeanloz R, Hanfland M and Taylor R D 2007 *Phys. Rev.* B **75** 020102
[15] Kobayashi H 2006 *Phys. Rev.* B **73** 104110
[16] Haavik C *et al* 2000 *Am. Mineral.* **85** 514
[17] Kuriki A *et al* 2002 *J. Phys. Soc. Japan* **71** 3092
[18] Ovsyannikov S V, Shchennikov V V, Todo S and Uwatoko Y 2008 *J. Phys.: Condens. Matter* **20** 172201
[19] Baudelet F, Pascarelli S, Mathon O, Itie J P, Polian A and Chervin J C 2010 *Phys. Rev.* B **82** 140412
[20] Brabers V A M 1971 *J. Cryst. Growth* **8** 26
[21] Miles P A, Westphal W B and Von Hippel A 1957 *Rev. Mod. Phys.* **29** 279
[22] Leonov I and Yaresko A N 2007 *J. Phys.: Condens. Matter* **19** 021001
[23] Mao H K, Xe J and Bell P M 1986 *J. Geophys. Res.* **91** 4673
[24] Schlegel A, Alvarado S F and Wachter P 1979 *J. Phys. C: Solid State Phys.* **12** 1157
[25] Degiorgi L, Blatter M I and Wachter P 1987 *Phys. Rev.* B **35** 5421
[26] Gasparov L V, Tanner D B, Romero D B, Berger H, Margaritondo G and Forro L 2000 *Phys. Rev.* B **62** 7939
[27] Pashkin A, Dressel M and Kuntscher C A 2006 *Phys. Rev.* B **74** 165118
[28] Ebad-Allah J, Baldassarre L, Sing M, Claessen R, Brabers V A M and Kuntscher C A 2009 *High Press. Res.* **29** 500
[29] Waldron R D 1955 *Phys. Rev.* **99** 1727
[30] Brabers V A M 1969 *Phys. Status Solidi* b **633** 563
[31] Kuntscher C A, Van der Marel D, Dressel M, Lichtenberg F and Mannhart J 2003 *Phys. Rev.* B **67** 035105
[32] Frank S, Kuntscher C A, Loa I, Yamauchi K and Lichtenberg F 2006 *Phys. Rev.* B **74** 054105 and references therein
[33] Thirunavukkuarasu K, Lichtenberg F and Kuntscher C A 2006 *J. Phys.: Condens. Matter* **18** 9173
[34] Kuntscher C A, Frank S, Loa I, Syassen K, Lichtenberg F, Yamauchi T and Ueda Y 2006 *Infrared Phys. Technol.* **49** 88
[35] Phuoc V Ta, Sellier C, Corraze B, Janod E and Marin C 2009 *Eur. J. Phys.* B **69** 181
[36] Emin D 1993 *Phys. Rev.* B **48** 13691
[37] Kuntscher C A, Frank S, Loa I, Syassen K, Yamauchi T and Ueda Y 2005 *Phys. Rev.* B **71** 220502
[38] Fratini S and Ciuchi S 2006 *Phys. Rev.* B **74** 075101
[39] Piekarz P, Parlinski K and Oles A M 2007 *Phys. Rev.* B **76** 165124
[40] Fratini S, de Pasquale F and Ciuchi S 2001 *Phys. Rev.* B **63** 153101
[41] Mott N F and Davis E A 1971 *Electronic Processes in Noncrystalline Materials* (Oxford: Clarendon)
[42] Kimura M *et al* 2010 *J. Phys. Soc. Japan* **79** 064710
[43] Frank S, Kuntscher C A, Gregora I, Petzelt J, Yamauchi T and Ueda Y 2007 *Phys. Rev.* B **76** 075128
[44] Rabia K, Pashkin A, Frank S, Obermeier G, Horn S, Hanfland M and Kuntscher C A 2009 *High Press. Res.* **29** 504